

Parallel Screening of Electrocatalyst Candidates Using Bipolar Electrochemistry

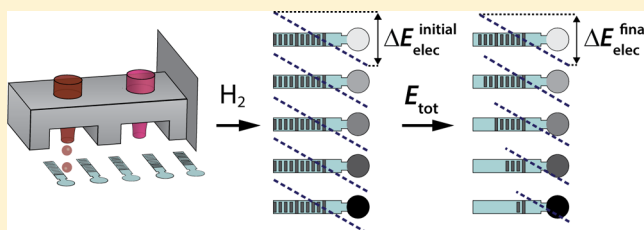
Stephen E. Fosdick,[†] Sean P. Berglund,[‡] C. Buddie Mullins,^{†,‡} and Richard M. Crooks^{*,†}

[†]Department of Chemistry and Biochemistry and the Center for Nano- and Molecular Science and Technology, The University of Texas at Austin, 105 E. 24th Street, Stop A5300, Austin, Texas 78712-1224, United States

[‡]McKetta Department of Chemical Engineering, The University of Texas at Austin, 200 E. Dean Keeton Street, Stop C0400, Austin, Texas 78712-1589, United States

S Supporting Information

ABSTRACT: Here we report simultaneous screening of bimetallic electrocatalyst candidates for the oxygen reduction reaction (ORR) using bipolar electrochemistry. The analysis is carried out by dispensing different bimetallic precursor compositions onto the cathodic poles of an array of bipolar electrodes (BPEs) and then heating them in a reducing atmosphere to yield the catalyst candidates. Because BPEs do not require a direct electrical connection for activation, up to 33 electrocatalysts can be screened simultaneously by applying a voltage to the electrolyte solution in which the BPE array is immersed. The screening of the electrocatalyst candidates can be achieved in about 10 min. The current required to drive the ORR arises from oxidation of Cr microbands present at the anodic poles of the BPEs. Therefore, the most effective electrocatalysts result in oxidation (dissolution) of the most microbands, and simply counting the microbands remaining at the end of the screen provides information about the onset potential required to reduce oxygen. Here, we evaluated three Pd–M (M = Au, Co, W) bimetallic electrocatalysts. In principle, arbitrarily large libraries of electrocatalysts can be screened using this approach.



Here we report the rapid screening of bimetallic electrocatalyst candidates for the oxygen reduction reaction (ORR) using bipolar electrochemistry.¹ The important new result is that arrays of catalyst candidates can be screened in a highly parallel format that requires only simple instrumentation: a microscope and a direct current (DC) power supply. As illustrated in Scheme 1a, the bipolar electrode (BPE) screening devices consist of indium tin oxide (ITO) electrodes having Cr microbands deposited at their anodic poles. Bimetallic catalyst candidates for the ORR are dispensed onto the cathodic poles. During a screening experiment, the BPE arrays are immersed in an acidic electrolyte solution, and a potential bias is applied between two driving electrodes positioned at either side of the array. The most effective catalyst candidates result in electrodisolution of the largest number of Cr microbands. Using this approach, we evaluated three potential bimetallic ORR electrocatalysts: Pd–Au, Pd–Co, and Pd–W.

One approach for discovering effective electrocatalysts is to rapidly evaluate large libraries of potential candidates.^{2,3} Promising materials identified during this preliminary screening step can then be subjected to more extensive and quantitative testing. Several techniques have been reported for rapid electrocatalyst screening. One of the first high-throughput methods was reported by Smotkin, Mallouk, and co-workers to screen for methanol-oxidation electrocatalysts. They used inkjet printing to define candidate materials on carbon paper and a pH-sensitive fluorescent indicator to reveal the most

effective catalysts.⁴ Other approaches make use of individually addressable working electrodes where the current passing through each electrode is monitored more or less simultaneously.^{5–8} The advantage of this method is that electrochemical parameters, such as kinetics, can be measured directly, but the cost for this additional information is increased complexity and smaller libraries.^{5,7} An approach pioneered by Bard and co-workers uses scanning electrochemical microscopy (SECM) to identify potential catalysts.^{9,10} Similar scanned-probe techniques have been reported for identifying photoelectrocatalysts by using either a rastered laser beam or optical fiber.^{11,12} These scanned probe techniques can be information rich, but they are usually rather slow as each array element is evaluated in serial rather than parallel. Finally, Tao and co-workers recently reported an approach that takes advantage of changes in the local refractive index of the electrolyte solution that arise from products of electrocatalytic reactions (for example, hydrogen evolution), which can be measured using surface plasmon resonance (SPR) microscopy.¹³

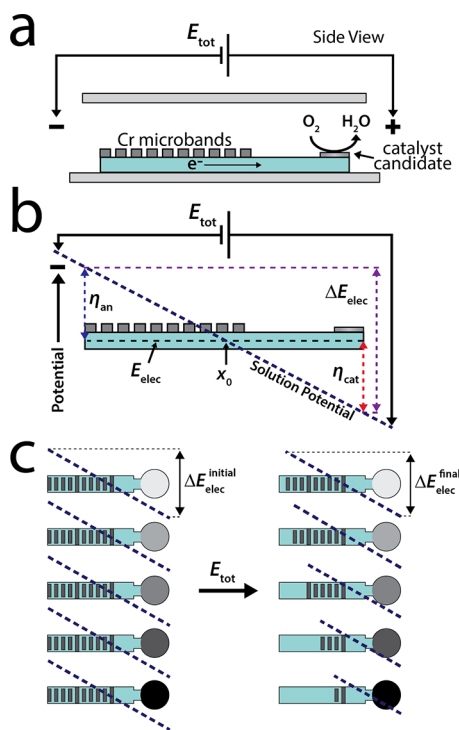
We recently introduced an electrocatalyst screening technique based on bipolar electrochemistry, where the electrodisolution of an array of thin metal microbands at the anodic pole of a BPE serves as an optical reporter of the

Received: December 10, 2012

Accepted: January 20, 2013

Published: February 6, 2013

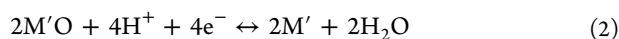
Scheme 1



performance of the catalyst immobilized on the cathodic pole.¹⁴ BPEs have a number of desirable characteristics for parallel screening of electrocatalysts. First, because arbitrarily large arrays of BPEs can be powered by a single pair of driving electrodes, individual electrodes in the array do not require a direct electrical connection.^{1,15–17} Second, each BPE in an array can be selectively modified with a different electrocatalyst candidate.^{14,18} Finally, the current passing through a BPE can be indirectly monitored using an optical readout based on either electrogenerated chemiluminescence (ECL)^{15,19} or electrodisolution of a thin metal film.^{14,20,21}

Other groups have reported screening techniques based on bipolar electrochemistry, but they make use of “closed” bipolar electrodes.²² For example, Zhang and co-workers very recently demonstrated a technique wherein an electrogenerated fluorescent probe is used to follow an electrocatalytic reaction.²³ In this configuration, BPEs provide the only electrical connection between two half cells.²⁴ Closed BPEs provide some advantages; for example, the two half cells may contain incompatible solutions, but it is difficult to ensure that the interfacial potential is the same for each electrode. The experiments reported in the present paper employ “open” BPEs, which reduce the magnitude of faradaic depolarization and minimize crosstalk between electrodes within the array.^{19,25}

The selection of the bimetallic catalyst candidates used in this study is based on thermodynamic guidelines proposed by Bard and co-workers.^{10,26,27} This approach focuses on the direct mechanism of the ORR (eqs 1 and 2).



In this scheme, molecular O_2 dissociates to yield adsorbed O (O_{ads}), and then O_{ads} is electroreduced to form H_2O . The guidelines suggest choosing a bimetallic system consisting of one metal (M) having a high $-\Delta G^\circ$ for the formation of a

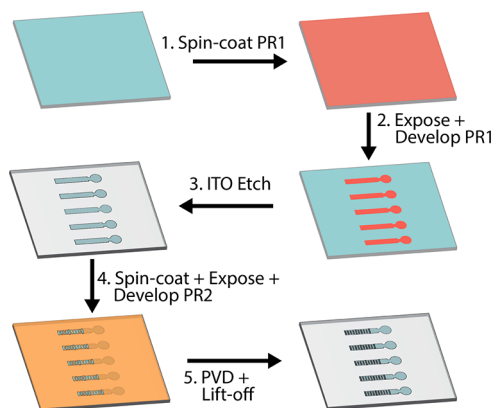
metal oxide (eq 1) and a second metal (M') that provides a positive standard potential for the reduction of the metal oxide (eq 2). Using these guidelines, we show that BPEs can be used to screen different ratios of three bimetallic compositions: Pd–Au, Pd–Co, and Pd–W. We chose these combinations for this first study, because, within the context of these guidelines, they provide distinct cases. Pd–Au does not adhere to the basic guidelines proposed by Bard and co-workers, because both Pd and Au are noble metals. Co and W represent species that readily form their respective oxides, with W having a more negative ΔG° for the reaction expressed by eq 1 than Co, -300 and -220 kJ/mol, respectively. Finally, combining Pd with Co or W adheres to the guideline, with Co and W facilitating eq 1 and Pd promoting eq 2. The standard potential of eq 2 for Pd is 0.92 V vs NHE.²⁸

EXPERIMENTAL SECTION

Chemicals. The following chemicals were used as received unless otherwise noted in the text: $(NH_4)_2PdCl_4$ (99.995%, Sigma Aldrich), $HAuCl_4 \cdot 3H_2O$ (99.9%, Sigma Aldrich), $Co(NO_3)_2 \cdot 6H_2O$ (99%, Fluka), $(NH_4)_6H_2W_{12}O_{40} \cdot xH_2O$ ($\geq 98.5\%$, Fluka), H_2SO_4 ($\geq 95\%$, trace analysis grade, Fluka), and ethylene glycol (99+%, Fisher Scientific). All aqueous solutions were prepared using Milli-Q water ($18.2 \Omega \cdot cm$). The concentration of the metal precursor solutions was 0.30 M (metal equivalent), and they were prepared in ethylene glycol.

Device Fabrication. ITO-coated glass slides ($4-8 \Omega/sq$) (Delta Technologies, Loveland, CO) were patterned using standard photolithographic methods as shown in Scheme 2.

Scheme 2

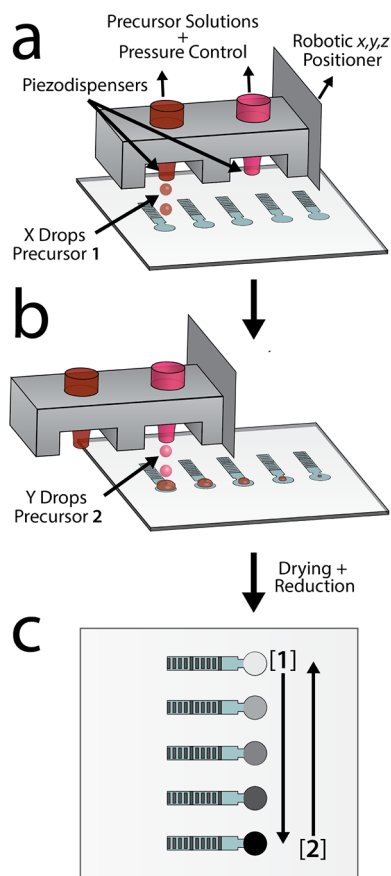


The slides were cleaned by sonication (15 min each in 1% Triton-X 100 in water, water only, and ethanol). A positive-tone photoresist layer (PR1) ($\sim 10 \mu m$ thick, AZ P4620) was then spin-coated onto the ITO-coated slides and exposed to UV light through a photomask. The unmasked PR1 layer was removed in a developer solution. The pattern was transferred to the ITO layer by a plasma-assisted reactive ion etch (Oxford Instruments Plasma Lab 80+). Next, the protective PR1 layer was removed using acetone, and the device was cleaned by sonication in 1% Triton-X, water, and ethanol. A negative lift-off photoresist (PR2) ($\sim 0.5 \mu m$ -thick, ma-N 1405, MicroChem Corp., Newton, MA) was deposited by spin-coating, exposed to UV light under a negative mask, and developed to remove photoresist over portions of the BPE anode. A 5 nm-thick layer of Cr was deposited by physical vapor deposition (PVD) over the devices. The unwanted Cr was removed by lift-off

(dissolution in acetone), leaving the microband array at each BPE anode. The devices were cleaned via sonication and dried under N_2 prior to dispensing precursor salts on the BPE cathodes. Each BPE is 2.50 mm long, with a 325 μm -diameter disk comprising the cathode. The lateral spacing of BPEs in the array is 750 μm center to center. The functional anode of each BPE consists of 70 individual Cr microbands (10 μm microbands and 10 μm edge-to-edge spacing). This device design was selected because crosstalk between neighboring electrodes was expected to result in less than 1% deviation in current flow at each electrode, as determined by finite-element simulations (Figure S1 in the Supporting Information).

Catalyst Candidate Preparation. The preparation of electrocatalyst candidates is depicted in Scheme 3. Precursor

Scheme 3



solutions were dispensed onto the cathodic poles of the BPEs in the array using a previously described robotic positioner/piezo-jet controller (CHI 1560A, CH Instruments, Austin, TX) fitted with a printhead assembly (PH046H-AT, Microfab, Plano, TX) containing four piezodispensers (80 μm tip diameter, Microfab).²⁹ The electrodes were aligned under the printhead using an x,y,z -micropositioner, and the dispensing alignment and progress were monitored via a USB microscope placed under the stage. The arrays were spotted using a total of 10 drops (~ 300 pL/drop) of the precursor solutions to maintain the total number of moles of metal constant on each electrode. The compositions were varied by changing the number of drops of each precursor solution (10–0, 9–1, ..., 1–9, 0–10). These compositional variations require 11 electrodes to produce the full range. Accordingly, each BPE device

includes 3 rows of 11 electrodes, allowing each composition to be simultaneously screened in triplicate.

The dispensed precursor solutions were dried in a vacuum oven (70 $^{\circ}\text{C}$) for 5 min to promote even coverage of metal precursors over the surface of the BPE cathode. The spotted materials were then reduced in flowing gas (5% $\text{H}_2/95\%$ N_2) for 1.5 h at 350 $^{\circ}\text{C}$. The effects of heating to this temperature were determined to have no deleterious effects on the ITO substrates (Supporting Information Figure S2). Supporting Information Figure S3 shows the spotting accuracy achieved for 256 electrodes used in this study.

BPE Array Screening. After chemical reduction of the precursor spots, the arrays were placed into a bipolar electrochemical cell (Supporting Information Figure S4). The cell uses two 0.5 mm-thick silicone gaskets as channel walls, which are placed between the slide containing the BPE array (top) and a microscope slide (bottom) (25 \times 36 mm). Glassy carbon (GC) driving electrodes were placed on top of the bottom substrate and ~ 2.5 mm from the edge of the device to prevent bubbles from entering in the channel. A voltage was applied between the two GC driving electrodes to produce the electric field in the bipolar electrochemical cell. The width of the microfluidic space was 1 cm for all experiments, and the volume of the resulting cell was ~ 125 μL . Screening of the BPE arrays was started within 5–6 min of the addition of air-saturated, 0.10 M H_2SO_4 electrolyte solution. $E_{\text{tot}} = 15.0$ V was applied for 5 min using a DC power supply (Lambda LLS9120, TDK-Lambda, Neptune, NJ). Finally, the cell was disassembled and the BPEs were gently rinsed with water and dried under N_2 .

The arrays were imaged using a Canon EOS Rebel T3i digital single-lens reflex (DSLR) camera connected to a Nikon AZ100 microscope using a Varimag II adapter (CNC Supply, Cape Coral, FL). The DSLR camera provides greater spatial resolution (full frame = 5824 \times 3456 pixels) than a traditional CCD camera, but at the expense of rapid image capture (1–3 fps). With this system, 10 μm features can be resolved over a field of view of ~ 9 mm \times 5 mm. Images were processed using ImageJ software (NIH, Bethesda, MD).

Compositional Analysis. The elemental compositions of deposited materials were determined using a scanning electron microscope (SEM) fitted with an energy dispersive X-ray analyzer (EDS). The SEM-EDS used in this study was a Quanta 650 FEG ESEM system with a Bruker XFlash 5010 EDS detector. Bimetallic spots were first prepared on naked ITO to ensure reproducible dispensing. Examples of the resulting test spots are shown in a series of micrographs in Supporting Information Figures S8–S10. SEM-EDS analysis of screened materials was achieved by grounding the BPEs to the SEM sample holder with a thin strip of carbon tape.

RESULTS AND DISCUSSION

Operating Principles of the BPE Screening System.

The operating principles of BPEs have been described previously¹ but are briefly reviewed here. A BPE is an electrically conductive material that responds to an electric field applied to an electrolyte solution by an external power supply (E_{tot} , Scheme 1a). In the absence of a direct electrical connection, the BPEs float to an equilibrium potential (E_{elec}) which is equal to the solution potential above the BPE at a certain point (x_0) along the electrode's length. When the electric field in solution is sufficiently high, faradaic reactions occur at the poles of the BPE. This is because the interfacial

potential differences, or overpotentials (η), between the electrode and solution vary across the length of the electrode. The BPE experiences both anodic (η_{an}) and cathodic (η_{cat}) overpotentials, with the highest overpotentials appearing at the extremities (Scheme 1b). The fraction of E_{tot} that is dropped over each electrode (ΔE_{elec}) depends on the length of the BPE relative to the length of the fluidic channel (l_{channel} , eq 3).

$$\Delta E_{\text{elec}} = E_{\text{tot}} \left(\frac{l_{\text{elec}}}{l_{\text{channel}}} \right) \quad (3)$$

In the experiments reported here, we take advantage of this relationship to evaluate electrocatalyst candidates. As shown in Scheme 1a, the application of a sufficiently high E_{tot} powers electrically coupled faradaic reactions at the BPE: the electrodisolution of Cr microbands and the ORR at the catalyst candidates. The highest overpotentials occur at the extreme ends of each BPE (Scheme 1b), meaning that the first microband to dissolve is the one closest to the edge of the BPE anode. In a microband dissolution experiment, the effective length of each BPE decreases as the number of microbands eliminated increases.^{14,20,21} This means that the overpotentials available to drive the two electrochemical reactions decrease over the course of the experiment and the rate of dissolution (and current) becomes very small, such that it effectively ceases. Because the electrochemical behavior of Cr oxidation is the same for each microband in the array, it is possible to estimate the relative onset potentials ($E_{\text{onset}}^{\text{ORR}}$) for each catalyst candidate by counting the number of Cr microbands that dissolve. The use of Cr microbands, rather than a continuous Cr film, simplifies the analysis of the experimental results.

Preliminary Testing of the BPE Array. For meaningful results to emerge from this type of screening study, it is essential that the electric field within the device be uniform. Accordingly, we carried out the following experiment to test this important point. First, a naked electrode array (no catalyst candidates) was configured within the bipolar electrochemical cell. Second, the cell was filled with 5.0 mM *p*-benzoquinone (BQ), which is readily reduced on unmodified ITO BPEs. BQ is a convenient species for control studies as the onset potential difference between BQ reduction and Cr oxidation is nearly 1 V (Supporting Information Figure S5). Third, $E_{\text{tot}} = 15.0$ V was applied to the cell for 5 min. No additional electrodisolution of Cr was observed after this time, because at this point the BPEs have shortened such that ΔE_{elec} is insufficient to drive additional faradaic processes.

The results of this experiment are shown in Figure 1. Before application of the driving voltage (Figure 1a), all 70 Cr microbands are visible on each of the 11 BPEs shown. However, after the external voltage is applied, Figure 1b shows that a number of microbands at the bottom of each ITO strip have oxidized and dissolved. If the field is uniform, then the same number of Cr microbands should be removed from each BPE. Figure 1c is a histogram showing the number of Cr microbands removed from each of the 33 BPEs in the array. The average number of bands eliminated is 20.9 ± 0.5 , which corresponds to a precision of 2%. The key conclusion is that each of the 33 electrodes behaves nearly identically.

Another important outcome of this experiment is that because the E_{onset} for BQ reduction and Cr electrodisolution, $E_{\text{onset}}^{\text{CrOx}}$ can be determined independently using a traditional 3-electrode electrochemical cell (Supporting Information Figure S5), it is possible to estimate the onset potentials for the ORR

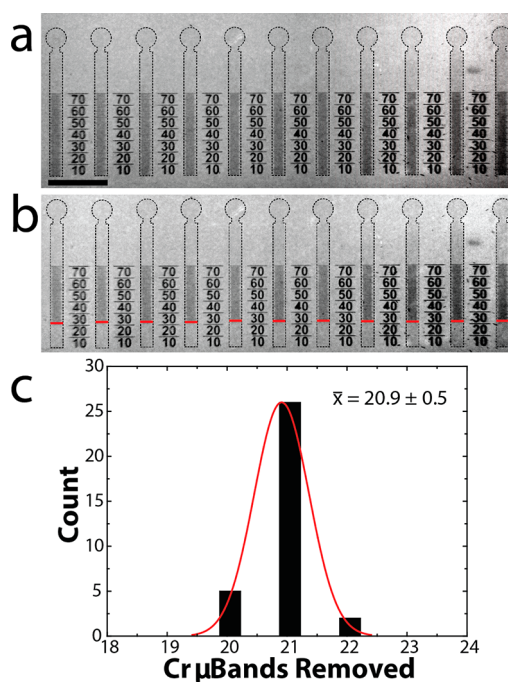


Figure 1. Results demonstrating the reproducibility of the BPE arrays used to screen catalysts. (a) Optical micrograph of a single row of 11 BPEs prior to electrochemical analysis. The black scale bar represents 1.0 mm. The ITO portions of the BPEs have been outlined (black dashed line) for clarity. (b) The array in part a after application of $E_{\text{tot}} = 15.0$ V for 5 min. The BPE cell was filled with a solution containing 5.0 mM BQ and 0.10 M H_2SO_4 . The red lines indicate the lowest microband on each BPE that did not undergo electrodisolution. (c) Histogram showing the number of Cr microbands dissolved for the 33 BPEs in the full array. The solid red line shows the normal distribution for this histogram.

in the bipolar electrochemical cell. Using eq 3 and the strength of the electric field, the value of ΔE_{elec} at the end of the experiment, $\Delta E_{\text{elec}}^{\text{final}}$ can be calculated by counting the number of Cr microbands eliminated and using the value of $E_{\text{onset}}^{\text{CrOx}}$ to determine $E_{\text{onset}}^{\text{ORR}}$ for each catalyst composition (eq 4).

$$E_{\text{onset}}^{\text{ORR}} \approx E_{\text{onset}}^{\text{CrOx}} - \Delta E_{\text{elec}}^{\text{final}} \quad (4)$$

This means that $E_{\text{onset}}^{\text{ORR}}$ for each species is directly related to the number of Cr microbands that dissolve during the screening experiment. We have directly measured the electric field in the bipolar electrochemical cell using a series of Au microbands patterned within the microfluidic space (Supporting Information Figure S6). The field is quite uniform and has a value of 0.46 V/mm. It is important to note that the values of $E_{\text{onset}}^{\text{ORR}}$ have been estimated using experimentally determined parameters. Therefore, they are most reliable for *comparing* the ORR onset potentials for the catalyst candidates examined in this study rather than as absolute values.

Screening Bimetallic Systems. Each BPE device is configured so that an array of bimetallic compositions can be screened in triplicate in <10 min. Figure 2 shows the outcome of a BPE screening experiment for 11 Pd–Co electrocatalyst compositions. Figure 2a is an optical micrograph of the array prior to the application of E_{tot} . The remaining frames show the evolution of the screening experiment at the times indicated in the individual frames. The red lines spanning the width of each BPE indicate the location of the bottom-most microband on each BPE that did not undergo electrodisolution. Movie S1 in

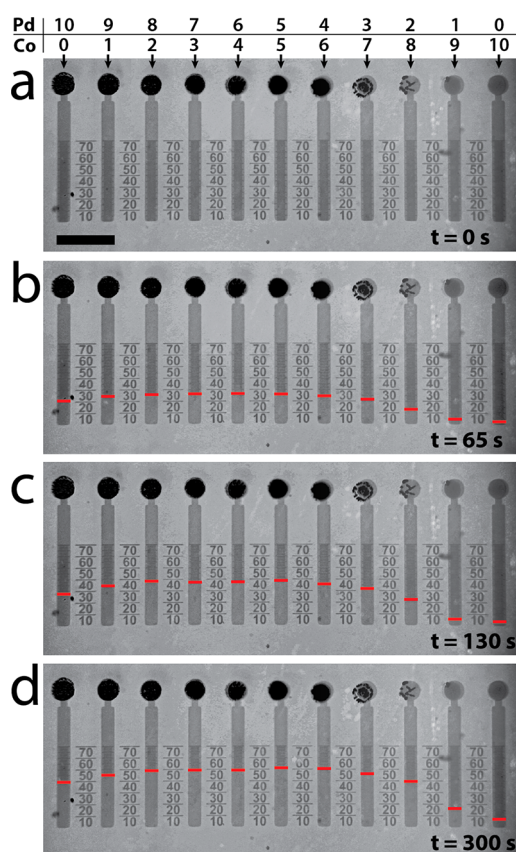


Figure 2. Optical micrographs representing a BPE ORR electrocatalyst screening experiment of different Pd–Co compositions. The electrode configuration is the same as that shown in Figure 1, except the cathodic poles of the BPEs have been modified with the different atomic ratios of Pd and Co indicated at the top of figure. The black scale bar represents 1.0 mm. The bipolar electrochemical cell was filled with $\sim 125 \mu\text{L}$ of air-saturated 0.10 M H_2SO_4 . (a) Prior to the application of a driving voltage. (b–d) After application of $E_{\text{tot}} = 15.0$ V for the times indicated in the bottom-right corner of each frame. The red lines show the position of the lowest microband on each BPE that did not undergo electrodisolution. These frames were extracted from Movie S1 in the Supporting Information. Figure S9 shows a series of SEM micrographs of the Pd–Co system, like that tested on this array.

the Supporting Information shows the entire screening experiment from which the frames in Figure 2 were extracted. The histograms in Figure 3 show the average number of Cr microbands removed for each composition of the three bimetallic electrocatalyst candidates examined in this study. The error bars represent the standard deviation from the mean obtained for a minimum of three independently prepared devices. That is, a total of at least nine screens for each composition.

The number of Cr bands oxidized for the 33 independently tested Pd-only electrocatalysts was 36.2 ± 3.9 . From this value and using eq 4, we estimate $E_{\text{onset}}^{\text{ORR}} = 0.46 \pm 0.04$ V vs reversible hydrogen electrode (RHE). A similar analysis indicates that $E_{\text{onset}}^{\text{ORR}}$ for pure Au is 0.17 ± 0.02 V vs RHE. In the case of the bimetallic Pd–Au electrocatalysts (Figure 2a), only a few of the compositions exhibit enhanced ORR activity compared to Pd-only. This is in accord with expectations based on the guidelines discussed earlier. For example, Pd₆–Au₄ revealed a statistically significant difference over Pd-only at the 95% confidence level. However, even in this case, the bimetallic only

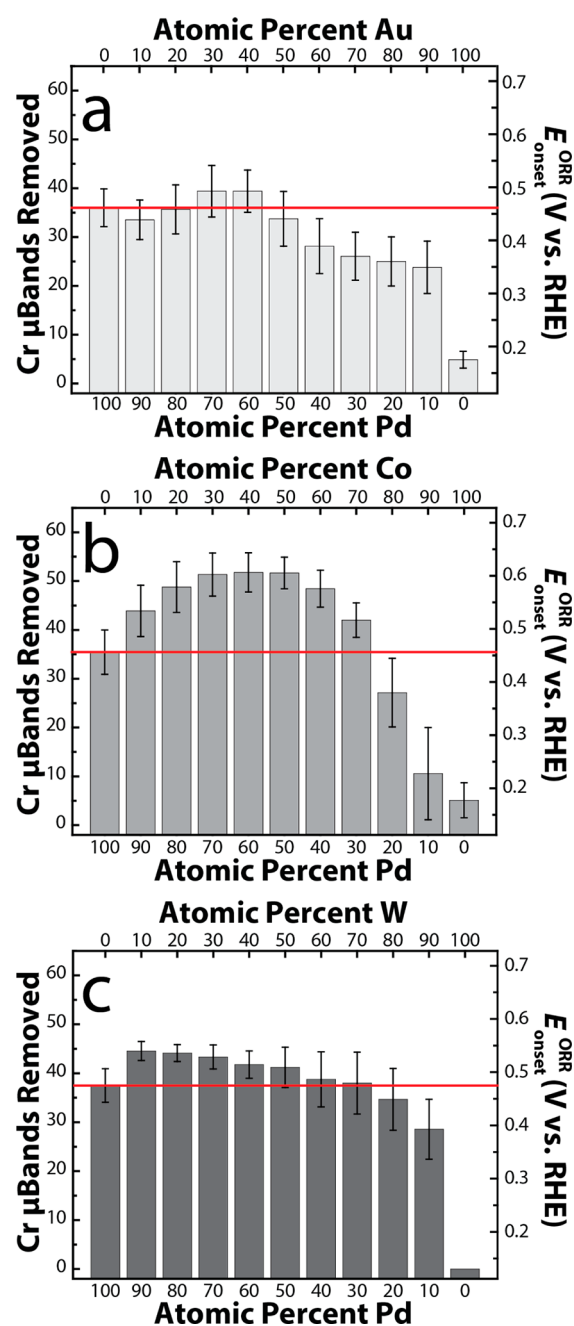


Figure 3. Histograms indicating the number of Cr microbands removed for each bimetallic composition tested: (a) Pd–Au, (b) Pd–Co, and (c) Pd–W. Each composition was tested in triplicate using at least nine separate BPEs. The error bars represent one standard deviation from the mean for each composition. The solid red lines indicate the performance of the 100% Pd electrocatalyst.

resulted in three more oxidized bands, which is equivalent to less than a 50 mV difference in $E_{\text{onset}}^{\text{ORR}}$.

A number of factors could be responsible for the $\sim \pm 10\%$ variation indicated by the error bars in Figure 3. First, the electrocatalyst candidates produced by the piezodispensing/ H_2 -reduction process are heterogeneous. SEM micrographs highlighting this observation are provided in the Supporting Information (Figures S8, S9, and S10). For example, micrographs of the Au-only catalyst reveal the presence of Au nanoparticles on the ITO support. This heterogeneity is important, because toward the end of each screening

experiment only the distal edge of the cathode of each BPE is active for the ORR (that is, only the longest dimension of the BPE is important). Heterogeneity in catalyst composition at this location will result in some scatter in the number of Cr microbands that dissolve. Second, for the same reason, slight differences in the location of the catalyst on the BPE cathode will also lead to some uncertainty in the results. In our experiments, the variation in the location of the spotted catalyst is approximately $\pm 30 \mu\text{m}$ in the direction parallel to the long axis of the electrodes (Supporting Information Figure S3).

Of the three bimetallic ORR electrocatalyst compositions studied, the Pd–Co materials exhibit the most positive shifts of $E_{\text{onset}}^{\text{ORR}}$ (Figure 3b). This result is consistent with those obtained by others using different electrochemical methods. For example, SECM results indicate that Pd₈–Co₂ is the most active composition for the ORR.^{10,26,30} Our data indicate that materials containing 30–90% Pd exhibit much more positive $E_{\text{onset}}^{\text{ORR}}$ values compared to pure Pd. For example, $E_{\text{onset}}^{\text{ORR}}$ for Pd₆–Co₄ is $0.61 \pm 0.04 \text{ V}$ vs RHE compared to $0.46 \pm 0.04 \text{ V}$ for the Pd-only catalyst. Several experimental and theoretical reports indicate that Pd–Co compositions ranging from Pd₉–Co₁ to Pd₆–Co₄ should show the greatest activity for the ORR.^{10,31–35}

It is important to point out here that the true identity of the most active phase in a certain compositional range is difficult to know with certainty (all electrochemical screening methods that rely on catalysts prepared by the method reported here suffer from this same problem). For example, as shown in Supporting Information Figure S9, the morphologies of the Pd–Co materials are quite heterogeneous even for a particular composition. Moreover, the Pd–Co system is not entirely stable in acidic electrolyte. In our experiments, dissolution of Co from the surface of the BPEs is apparent from micrographs collected during the screening experiments, and EDS results obtained after screening indicate a marked change in final composition (Supporting Information Figure S7b). For example, EDS analysis indicates that after screening the compositions of the Pd–Co bimetallics typically contain 60–90% Pd, depending on the initial percentage of Pd present. This compositional change accounts for the surprisingly high $E_{\text{onset}}^{\text{ORR}}$ for the catalysts having a nominally low percentage of Pd. The point is that loss of Co from the BPE cathodes increases the Pd:Co ratio but also lowers the overall metal loading, and these factors compromise the assumed catalyst structure–function relationship to some extent.

The Pd–W bimetallics (Figure 3c) represent the most extreme differences in the $-\Delta G^\circ$ values for the reaction shown in eq 2, and the standard reduction potential for the reaction shown in eq 3 for the two materials. As has been shown previously, the presence of W in bimetallic compositions containing 50–90% Pd does result in some improvement in electrocatalytic behavior compared to the Pd-only catalyst.³⁶ Like the Pd–Co catalyst, the Pd–W system also exhibits some loss of W in the acidic electrolyte. However, this effect is much less pronounced for the Pd–W electrocatalyst (Supporting Information Figure S7b).

Optical Determination of Current. Thus far we have only discussed the total number of microbands remaining at the end of a screening experiment and, then, correlated these data to the onset potential of the ORR. This only requires a single micrograph, such as that shown in Figure 2d, obtained at the end of a screening experiment. However, one of the main virtues of this catalyst-selection method is that it is nearly as

straightforward to capture the time evolution of the entire BPE array in situ. For example, Figure 4 is a plot of the number of

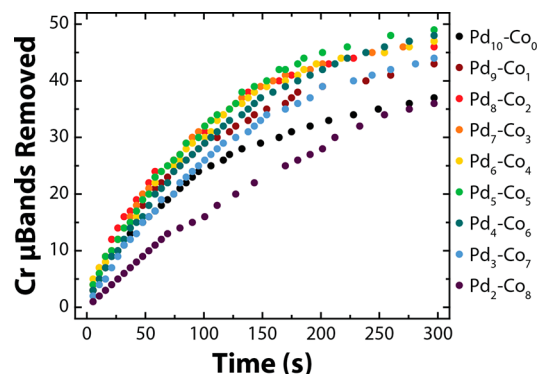


Figure 4. Plot of the number of Cr microbands removed vs time for one row of BPEs. These data were extracted from Movie S1 in the Supporting Information.

bands dissolved vs time for a BPE array spotted with different Pd–Co compositions. These data were extracted from Supporting Information Movie S1. Because each Cr microband represents a certain quantity of charge, it is possible to correlate such data to the current flowing through each BPE. In the future, we plan to show that quantitative kinetic information can be derived from these types of results using finite element simulations. For now, however, we content ourselves with the thermodynamic data presented in the previous section.

SUMMARY AND CONCLUSIONS

In this study, we have shown that bipolar electrochemistry provides a simple and highly parallel means for evaluating electrocatalyst candidates. To demonstrate this, we prepared 11 distinct compositions of each of three bimetallic electrocatalysts and tested their effectiveness for the ORR using arrays of wireless BPEs. The Pd–Co electrocatalyst proved to be the most effective. However, we showed that interpretation of these results requires caution due to catalyst instability and differences in the morphologies of the catalysts that depend on the relative amounts of the two metals present.

The methodology reported here provides a number of important advances over our earlier preliminary report of this general approach for electrocatalyst screening.¹⁴ First, the number of electrodes per screening platform has been increased by more than an order of magnitude, which means more materials can be screened per experiment. It is also important to note that the device design can easily be changed to accommodate much larger arrays. Here, because we wanted to capture real-time, in situ movies of the electrodisolution of the Cr microbands, the size of the array was limited by the resolution and field-of-view of our microscope and camera. Second, we have implemented piezodispensing as a means of producing arrays of materials of varying compositions. Third, we changed the identity of the reporter from Ag to Cr, because Cr requires a more positive potential to oxidize (near the thermodynamic potential of the ORR), meaning that materials requiring low overpotentials for the ORR can be reliably evaluated. The potential needed to oxidize Ag can actually be negative with respect to the ORR for certain promising catalyst candidates, meaning that the ORR and Ag oxidation could take place spontaneously (prior to the application of E_{tot}). The switch from Ag to Cr has several other benefits, such as simpler

microfabrication and less risk of poisoning catalyst candidates with an easily reducible species such as Ag^+ .

There are limitations to this technique in its current form. First, preparation of the platform requires fairly sophisticated microfabrication. Second, the electrode density (number of BPEs/cm²) is limited by the method used to dispense the electrocatalysts. Third, it is important to control the location of the electrocatalysts. Fourth, the ITO substrate limits the maximum annealing temperature of the dispensed precursors. To varying degrees, there are probably solutions to all of these problems, and as the methodology evolves we will report on such advances. Finally, as for all such screening methods, variations in morphology of multimetallic catalyst candidates make it difficult to unambiguously identify the active phase.

Looking to the future, we plan to develop simulation tools to extract kinetic information using data like that shown in Figure 4. We also plan to expand the number of catalyst candidates that can be simultaneously screened by using inkjet printing rather than the current method. Inkjet printing is capable of dispensing submicrometer spot sizes.³⁷ Accordingly, we anticipate increasing the size of the array to hundreds (or even thousands) of BPEs, which can be screened in just a few minutes.

■ ASSOCIATED CONTENT

📽 Supporting Information

Movie of the screening experiment for Pd–Co system, finite element simulations for electrode crosstalk, information about effects of heat treatment on ITO, photograph of the bipolar electrochemical cell, plot of spotting accuracy, three-electrode experiments for Cr dissolution and BQ reduction, electric field measurements, and SEM-EDS analysis. This material is available free of charge via the Internet at <http://pubs.acs.org>.

■ AUTHOR INFORMATION

Corresponding Author

*E-mail: crooks@cm.utexas.edu.

Notes

The authors declare no competing financial interest.

■ ACKNOWLEDGMENTS

S.E.F. and R.M.C. gratefully acknowledge financial support from the Chemical Sciences, Geosciences, and Biosciences Division, Office of Basic Energy Sciences, Office of Science, U.S. Department of Energy (contract no. DE-FG02-06ER15758). The Robert A. Welch Foundation provides sustained support for our research (Grant F-0032 for R.M.C. and F-1436 for C.B.M.). S.P.B. thanks the National Science Foundation for a Graduate Fellowship. We also thank James A. Loussaert for help with XPS measurements.

■ REFERENCES

- (1) Mavr , F.; Anand, R. K.; Laws, D. R.; Chow, K.-F.; Chang, B.-Y.; Crooks, J. A.; Crooks, R. M. *Anal. Chem.* **2010**, *82*, 8766–8774.
- (2) Smotkin, E. S.; D az-Morales, R. R. *Annu. Rev. Mater. Res.* **2003**, *33*, 557–579.
- (3) Jeon, M. K.; Lee, C. H.; Park, G. I.; Kang, K. H. *J. Power Sources* **2012**, *216*, 400–408.
- (4) Reddington, E.; Sapienza, A.; Gurau, B.; Viswanathan, R.; Sarangapani, S.; Smotkin, E. S.; Mallouk, T. E. *Science* **1998**, *280*, 1735–1737.
- (5) Sullivan, M. G.; Utomo, H.; Fagan, P. J.; Ward, M. D. *Anal. Chem.* **1999**, *71*, 4369–4375.

- (6) Strasser, P.; Fan, Q.; Devenney, M.; Weinberg, W. H.; Liu, P.; N rskov, J. K. *J. Phys. Chem. B* **2003**, *107*, 11013–11021.
- (7) Guerin, S.; Hayden, B. E.; Lee, C. E.; Mormiche, C.; Owen, J. R.; Russell, A. E.; Theobald, B.; Thompsett, D. *J. Comb. Chem.* **2004**, *6*, 149–158.
- (8) Neyerlin, K. C.; Bugosh, G.; Forgie, R.; Liu, Z. C.; Strasser, P. *J. Electrochem. Soc.* **2009**, *156*, B363–B369.
- (9) Bard, A. J. *J. Am. Chem. Soc.* **2010**, *132*, 7559–7567.
- (10) Fern ndez, J. L.; Walsh, D. A.; Bard, A. J. *J. Am. Chem. Soc.* **2005**, *127*, 357–365.
- (11) Woodhouse, M.; Parkinson, B. A. *Chem. Mater.* **2008**, *20*, 2495–2502.
- (12) Ye, H.; Lee, J.; Jang, J. S.; Bard, A. J. *J. Phys. Chem. C* **2010**, *114*, 13322–13328.
- (13) Shan, X. N.; Diez-Perez, I.; Wang, L. J.; Wiktor, P.; Gu, Y.; Zhang, L. H.; Wang, W.; Lu, J.; Wang, S. P.; Gong, Q. H.; Li, J. H.; Tao, N. J. *Nat. Nanotechnol.* **2012**, *7*, 668–672.
- (14) Fosdick, S. E.; Crooks, R. M. *J. Am. Chem. Soc.* **2012**, *134*, 863–866.
- (15) Arora, A.; Eijkel, J. C. T.; Morf, W. E.; Manz, A. *Anal. Chem.* **2001**, *73*, 3282–3288.
- (16) Zhan, W.; Alvarez, J.; Crooks, R. M. *J. Am. Chem. Soc.* **2002**, *124*, 13265–13270.
- (17) Chow, K.-F.; Mavr , F.; Crooks, J. A.; Chang, B.-Y.; Crooks, R. M. *J. Am. Chem. Soc.* **2009**, *131*, 8364–8365.
- (18) Chow, K.-F.; Mavr , F.; Crooks, R. M. *J. Am. Chem. Soc.* **2008**, *130*, 7544–7545.
- (19) Mavr , F.; Chow, K.-F.; Sheridan, E.; Chang, B.-Y.; Crooks, J. A.; Crooks, R. M. *Anal. Chem.* **2009**, *81*, 6218–6225.
- (20) Duval, J. F. L.; Kleijn, J. M.; van Leeuwen, H. P. *J. Electroanal. Chem.* **2001**, *505*, 1–11.
- (21) Chow, K.-F.; Chang, B.-Y.; Zaccheo, B. A.; Mavr , F.; Crooks, R. M. *J. Am. Chem. Soc.* **2010**, *132*, 9228–9229.
- (22) Lin, X.; Zheng, L.; Gao, G.; Chi, Y.; Chen, G. *Anal. Chem.* **2012**, *84*, 7700–7707.
- (23) Guerrette, J. P.; Percival, S. J.; Zhang, B. *J. Am. Chem. Soc.* **2013**, *135*, 855–861.
- (24) Guerrette, J. P.; Oja, S. M.; Zhang, B. *Anal. Chem.* **2012**, *84*, 1609–1616.
- (25) Duval, J. F. L.; Huijs, G. K.; Threels, W. F.; Lyklema, J.; van Leeuwen, H. P. *J. Colloid Interface Sci.* **2003**, *260*, 95–106.
- (26) Fern ndez, J. L.; White, J. M.; Sun, Y. M.; Tang, W. J.; Henkelman, G.; Bard, A. J. *Langmuir* **2006**, *22*, 10426–10431.
- (27) Walsh, D. A.; Fern ndez, J. L.; Bard, A. J. *J. Electrochem. Soc.* **2006**, *153*, E99–E103.
- (28) Bard, A. J.; Parsons, R.; Jordan, J., Eds. *Standard Potentials in Aqueous Solutions*; Marcel Dekker: New York, 1985.
- (29) Berglund, S. P.; Lee, H. C.; Nu ez, P. D.; Bard, A. J.; Mullins, C. B. *Phys. Chem. Chem. Phys.* **2013**, submitted.
- (30) Lin, C.-L.; S nchez-S nchez, C. M.; Bard, A. J. *Electrochem. Solid-State Lett.* **2008**, *11*, B136–B139.
- (31) Yu, T. H.; Sha, Y.; Merinov, B. V.; Goddard, W. A. *J. Phys. Chem. C* **2010**, *114*, 11527–11533.
- (32) Lee, K. R.; Jung, Y.; Woo, S. I. *ACS Comb. Sci.* **2011**, *14*, 10–16.
- (33) Mustain, W. E.; Kepler, K.; Prakash, J. *Electrochim. Acta* **2007**, *52*, 2102–2108.
- (34) Koenigsmann, C.; Sutter, E.; Chiesa, T. A.; Adzic, R. R.; Wong, S. S. *Nano Lett.* **2012**, *12*, 2013–2020.
- (35) Shao, M.; Liu, P.; Zhang, J.; Adzic, R. *J. Phys. Chem. B* **2007**, *111*, 6772–6775.
- (36) Li, W.; Fan, F.-R. F.; Bard, A. J. *J. Solid State Electrochem.* **2012**, *16*, 2563–2568.
- (37) Singh, M.; Haverinen, H. M.; Dhagat, P.; Jabbour, G. E. *Adv. Mater.* **2010**, *22*, 673–685.